BACKSCATTERING BY A SPHERICAL ELASTIC SHELL CLOSE TO THE AIR-WATER INTERFACE: COMPARISON BETWEEN EXPERIMENT AND MODELLING

J-P Sessarego, CNRS/LMA Marseille, France
N S Grigorieva, St. Petersburg State Marine Technical University, St. Petersburg, Russia
P Cristini, CNRS/LMA Marseille, France
G M Fridman, St. Petersburg State Marine Technical University, St. Petersburg, Russia

1 INTRODUCTION

Acoustic wave scattering from elastic objects immersed in water yields information about the object that can be used for detection and identification. However, when objects are close to the air-water interface or close to the sea bottom, detection becomes much more difficult because of the local effects of the environment. These effects are essentially due to both interactions of the insonifying wave with the interface and object-interface interactions including multiple reflections of the scattered field. This problem was addressed by many authors, but detailed studies including modelling in frequency and time domains for different distances from the object to the interface, varying angles of insonification and different wide band pulses are not yet available. Moreover, in parallel with this modelling, carefully controlled experimental measurements are needed to test the used models, but these measurements are practically non existent.

In the present paper we examine in detail the backscattering by a spherical elastic shell close to the air-water interface and compare the obtained computational results with the data from a controlled experiment in a water tank. To make a quantitative comparison with experiments, we used a spherical elastic shell of thickness 4% of the outer radius. This shell was filled with air. The p-wave and s-wave speeds were obtained from the elastic modulus of the material given by the manufacturer, and density was measured in the laboratory. These values were confirmed by comparing the measured and calculated free field backscattering form functions in water. In order to insonify the shell, two wide band Panametrics transducers working at respectively 250 kHz (bandwidth: 120 kHz at -3dB) and 500 kHz (bandwidth: 250 kHz at -3dB) were used.

Numerical computations of the scattered field were made over a wide frequency range of $0<k_0a<60$ ($k_0=\omega/c_0$, a is the shell radius). In this frequency range, for a thin air-filled spherical shell, the elastic contribution to scattering is due to the lowest-order flexural and compressional waves of the shell. These waves may be considered as the generalization of the Lamb symmetric (or compressional) S_0 wave and the antisymmetric (or flexural) A_0 wave of a flat plate.

2 THE SOLUTION OF THE BACKSCATTERING PROBLEM IN THE FREQUENCY DOMAIN

The geometry of the problem is shown in Figure 1. The point source emitting the incident spherical wave is located in water, just beneath the air-water interface, at S(r, θ, 0) in the (r, θ, ϕ) spherical system of coordinates, and S=S (ρ, 0, z) in the cylindrical coordinate system. The problem of finding the backscattered field taking into account all the interaction effects between the object and air-water interface was examined in many papers. In the paper by Huang et al.[1] the solution was found by the method of images. However, we will use the T-matrix method[2] because it can be generalized to the case of an object near a seabed interface[3].

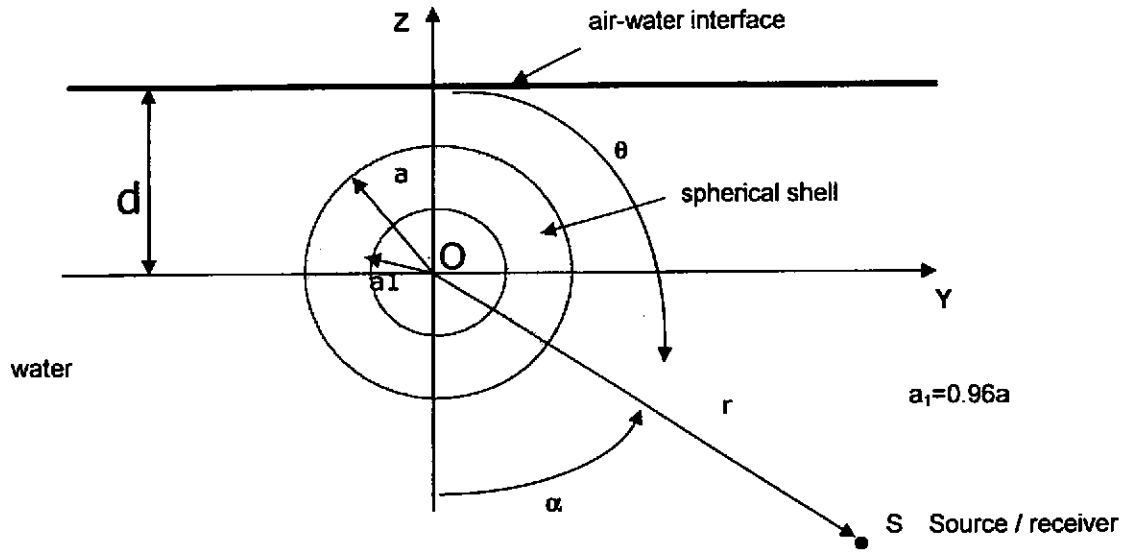

Figure 1. Scattering geometry

The total field observed at S can be represented in the form[2]

(1) $$\tilde{\Phi}_{total} = \tilde{\Phi}_{source} + \tilde{\Phi}_{scatterer},$$

where

(2) $$\tilde{\Phi}_{source} = -\frac{e^{2ik_0(d+r\cos\alpha)}}{8\pi(d+r\cos\alpha)}$$

is the spherical wave reflected from the interface, and

(3) $$\tilde{\Phi}_{scatterer} = -\frac{i}{k_0}\sum_{l=0}^{l_{max}}\sum_{m=0}^{l} A_{ml}(\vec{r})T_l c_{ml}$$

is the scattered field.

In Eq. (3), T_l are elements of the free-field **T** matrix for the acoustical scattering by a spherical shell. The truncation level l_{max} appearing in this formula was set by a rule suggested by Kargl and Marston[4] (see, also Ref. 5, p.1767)

$$l_{max} = [k_0 a + 4.05(k_0 a)^{1/3}] + 3,$$

where [x] is the integer part of x. The coefficients A_{ml} are given by the following relation:

(4) $$A_{ml}(\vec{r}) = i(\frac{\varepsilon_m}{2\pi})^{1/2}\int_0^{\infty}\frac{qdq}{h}J_m(q\rho)\left(e^{-ihz}B_{ml}(\frac{h}{k_0}) - e^{ih(2d-z)}B_{ml}(-\frac{h}{k_0})\right).$$

Here $\varepsilon_0=1$, $\varepsilon_m=2$ for $m \geq 1$, and $h = \sqrt{k_0^2 - q^2}$; $\mathrm{Im}(h) \geq 0$. J_m is the cylindrical Bessel function of the m-th order and

$$B_{ml}(\frac{h}{k_0}) = i^{l-m}\left(\frac{2l+1}{2}\frac{(l-m)!}{(l+m)!}\right)^{1/2} P_l^m(\frac{h}{k_0}),$$

where P_l^m is the associated Legendre function of order l and rank m.

Equation (4) can be written as the sum of two terms[3]:

$$A_{ml} = A_{ml}^{(f)} + A_{ml}^{(d)}.$$

The first summand is a single outgoing spherical harmonic of the field scattered from a target, written in the form of a plane wave decomposition. The second summand is the wave field resulting from the reflection of the (l, m) spherical harmonic off the air-water interface. It tends to zero as d tends to infinity.

Coefficients c_{ml} in Eq. (3) are found from a linear system of algebraic equations:

(5) $$c_{ml} = A_{ml}(\bar{r}) + i\sum_{l'=m}^{l'_{max}} R_{l,l'}^{m} T_{l'} c_{ml'},$$

where $l'_{max} = l_{max}$ and $0 \le m \le \min(l,l')$,

(6) $$R_{l,l'}^{m} = 2i\int_0^{\infty} \frac{qdq}{hk_0} B_{ml}(-\frac{h}{k_0}) B_{ml'}(-\frac{h}{k_0}) e^{2ihd}.$$

$R^{m}_{l,l'}$ is the conversion coefficient of the l-th outgoing harmonic into the l'-th incoming harmonic reflected from the air-water interface. It can be expressed via the Wigner 3j-symbols[3, 6, 7].

Finding of the coefficients c_{ml} at large k_0a is a very time consuming procedure, because of both the calculation of the Wigner 3j-symbols and the resolution of the system (5). In reality, to find the coefficients c_{ml}, it is necessary to solve $l_{max}+1$ systems of equations: a system of $l_{max}+1$ equations with $l_{max}+1$ unknowns at m=0, a system of l_{max} equations with l_{max} unknowns at m=1, etc..., and finally a system consisting of one equation with one unknown value $c_{l_{max}l_{max}}$ at m $=l_{max}$.

3 FREE FIELD COMPUTATION FOR A SPHERICAL SHELL AND COMPARISON WITH EXPERIMENTS

In notations used above, the backscattered free field of a spherical shell will be of the form:

(7) $$\tilde{\Phi}^{(f)}(\omega) = -\frac{i}{k_0}\sum_{l=0}^{l_{max}}\sum_{m=0}^{l} T_l (A_{ml}^{(f)}(\bar{r}))^2,$$

where

(8) $$A_{ml}^{(f)} = ik_0 h_l^{(1)}(k_0 r)\xi_{lm} P_l^m(-\cos\alpha).$$

In Eq. (8), $h_l^{(1)}$ is the spherical Hankel function of the first kind,

(9) $$\xi_{lm} = (\frac{\varepsilon_m (2l+1)(l-m)!}{4\pi(l+m)!})^{1/2}.$$

In order to compute the free field form function, we used the following expression:

(10) $$\left|F^{(f)}(\omega)\right| = \frac{8\pi r^2}{a}\left|\tilde{\Phi}^{(f)}(\omega)\right|,$$

where r is the distance to the field point and a is the outer radius of the object.

Computations were made for parameters of the spherical shell used in the experiments. This shell was made of an alloy composed of nickel and molybdenum. Physical parameters of this material are given in Table 1. A graph of the free field form function as a function of k_0a is shown in Figure 2. In this Figure we can observe several different domains. In particular, in the range $20<k_0a<35$ we can see a region of strong resonances which are directly connected with the well known antisymmetric Lamb wave A_0, and in the range $10<k_0a<20$ resonances related to the symmetric Lamb wave S_0. These resonances have been studied in detail by several authors during the last 20 years.

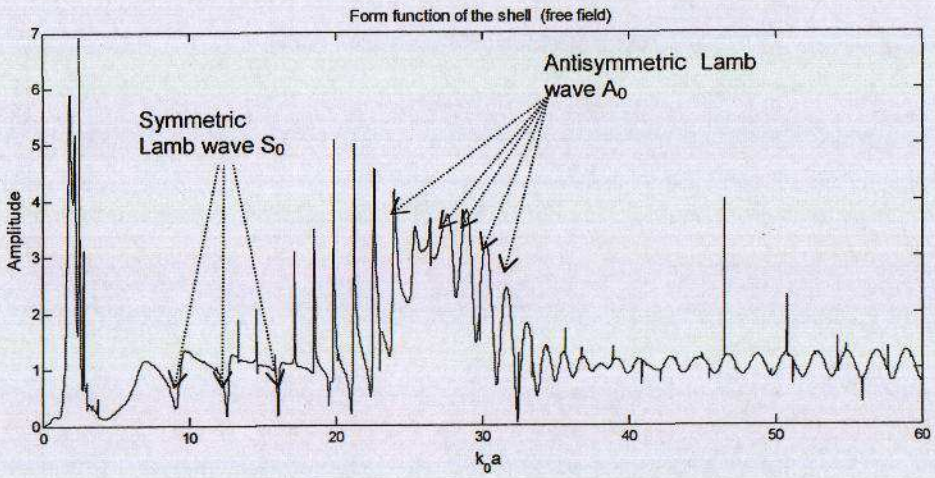

Figure 2. Form function of a spherical shell as a function of k_0a

P-wave speed	5554.5m/s
S-wave speed	3020.8m/s
Density	9217kg/m^3
Outer radius	1.5cm

Table I. Physical properties of the shell

3.1 Tank Experiments

In order to check our theoretical results, we made a quantitative comparison with an experiment in well controlled conditions. The physical properties of the shell are given in Table 1. The shell was placed just beneath the air-water interface. It was illuminated by two wide band transducers, the first one working at 250 kHz (BW=120 kHz at -3dB) and the second one at 500 kHz (BW=250 kHz at -3dB). The echoes were received by the transmitter/receiver system and recorded on a 40MHz A/D card. A photo of the tank used for this experiment is shown in Figure 3.

The carriage supporting the transducer can be moved in the X, Y and Z position with a high degree of accuracy, all the movements being controlled by stepping motors; the angular direction of the transducer itself can be changed by steps of 1/10° between 0° and 180°. This set-up allows a very accurate positioning of the transducer and target in the tank.

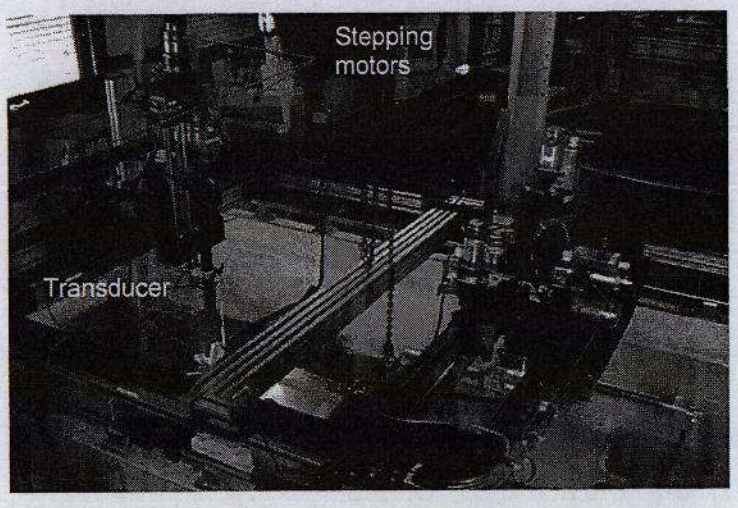

Figure 3. Photo of the tank used for the experiments

The digitized signals obtained from the experiment could not be used directly for comparison with theoretical curves. To make a comparison in the frequency domain, we first applied the inverse Fourier transform to these signals. The spectrum contains not only the information about target but it includes also the filtering effect of the transducer. In order to compare the theoretical form function with the echo spectrum, we have multiplied the form function by a window W(ω) taking into account the filtering effect of the transducers:

$$\left|F_w^{(f)}(\omega)\right| = \frac{8\pi r^2}{a}\left|\tilde{\Phi}^{(f)}(\omega).W(\omega)\right|. \tag{11}$$

3.2 Comparison Theory-Experiment For Free Field

The result of comparison is given in Figure 4a for transducer T1 and Figure 4b for transducer T2.

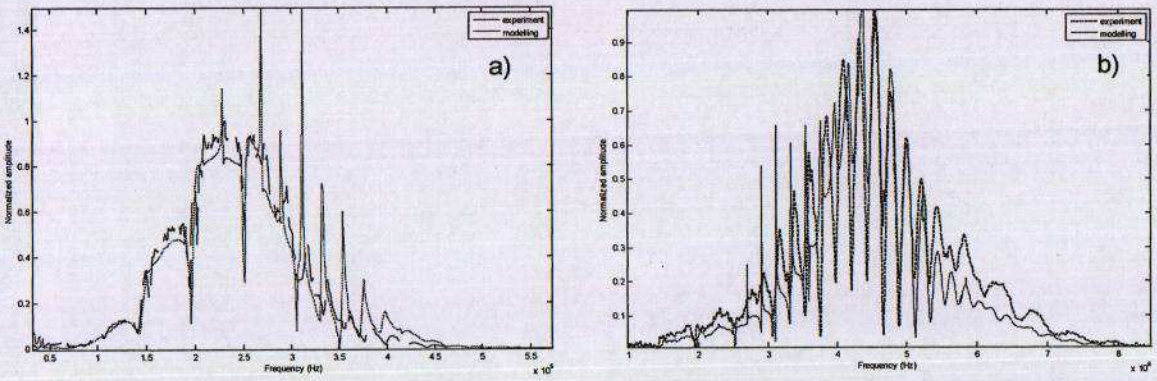

Figure 4. Comparison of the free field response of the shell: a) transducer T1 (250 kHz); b) transducer T2 (500 kHz)

These Figures show a good agreement between modelling and experiment. Except the very narrow spikes predicted by theory and which cannot be observed in the experiment, all the other resonances can be clearly seen.

In the time domain there is a good agreement for both frequencies (250 kHz and 500 kHz). The small differences observed on the amplitudes of signals are certainly due to some imperfection in the manufacturing of the shell, in particular in the welding of the two hemispherical caps. In the upper curve of Figure 5 we can observe different components which correspond to surface waves of the S_0

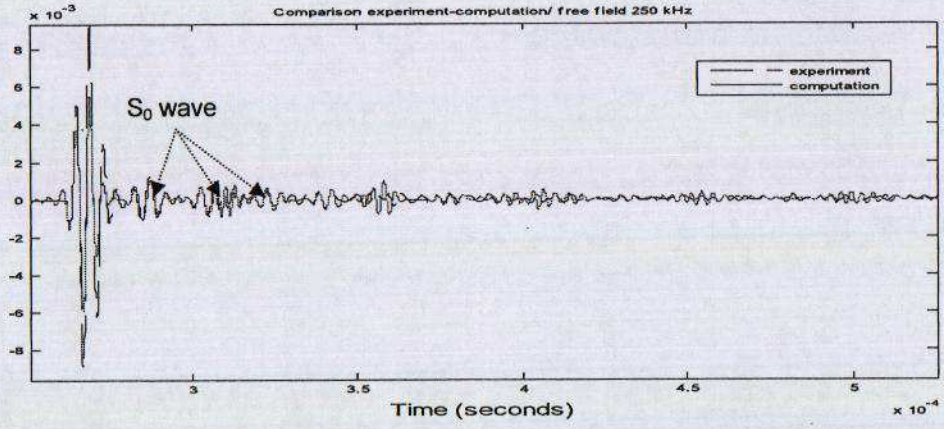

type. In the lower curve, surface waves of the A_0 type are clearly seen. They are dispersive as it is predicted by the theory and they appear with a repetition rate corresponding to a circumnavigation around the shell. For this comparison between experiment and calculation the ratio r/a was about 20 (r is the distance to the source and a is the radius of the object).

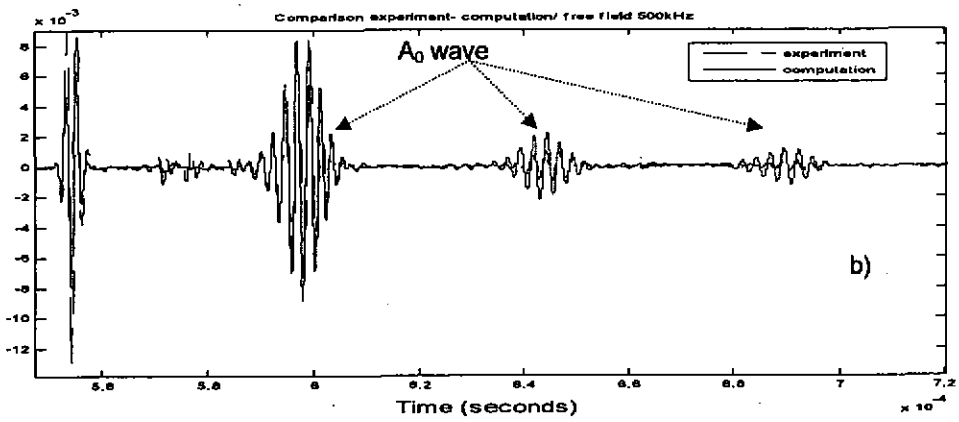

Figure 5. Echoes of the shell in free space received by: a) transducer T1, b) transducer T2

r/a~20

4 FULL FIELD COMPUTATION

We computed the scattered field for a spherical shell situated 1mm beneath the air-water interface. The calculation was performed for two angles of illumination in the range $0<k_0a<60$. From the scattered field

(12) $$\tilde{\Phi}_{scatterer} = -\frac{i}{k_0}\sum_{l=0}^{l_{max}}\sum_{m=0}^{l} A_{ml}(\vec{r})T_l\, c_{ml}$$

we find the form function

(13) $$\left|F_{scatterer}(\omega)\right| = \frac{8\pi r^2}{a}\left|\tilde{\Phi}_{scatterer}(\omega)\right|.$$

We computed also an approximation of the full scattered field by using the following assumption:

(14) $$c_{ml} = A_{ml}(\vec{r}).$$

In this case the scattered field can be calculated according the relation:

(15) $$\tilde{\Phi}_{scatterer} = -\frac{i}{k_0}\sum_{l=0}^{l_{max}}\sum_{m=0}^{l}\left(A_{ml}(\vec{r})\right)^2 T_l.$$

The approximation (15) takes into account the backscattered free field of a spherical shell as well as the field reflected from the air-water interface and then scattered from the target.
The results of computations are given in Figures 6 and 7 for the angles of incidence alpha=30° and alpha= 0°, respectively.

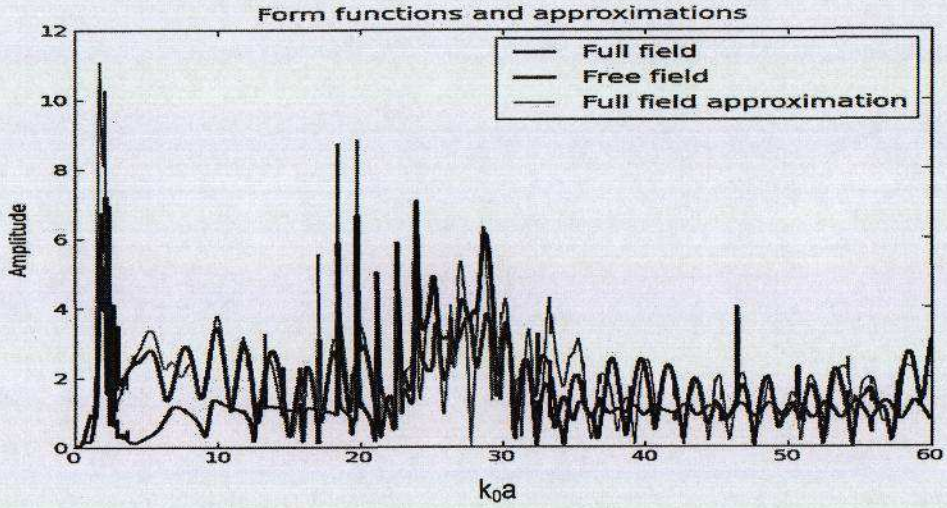

Figure 6. Computation of the form functions for a shell placed 1mm beneath the interface, alpha =30°

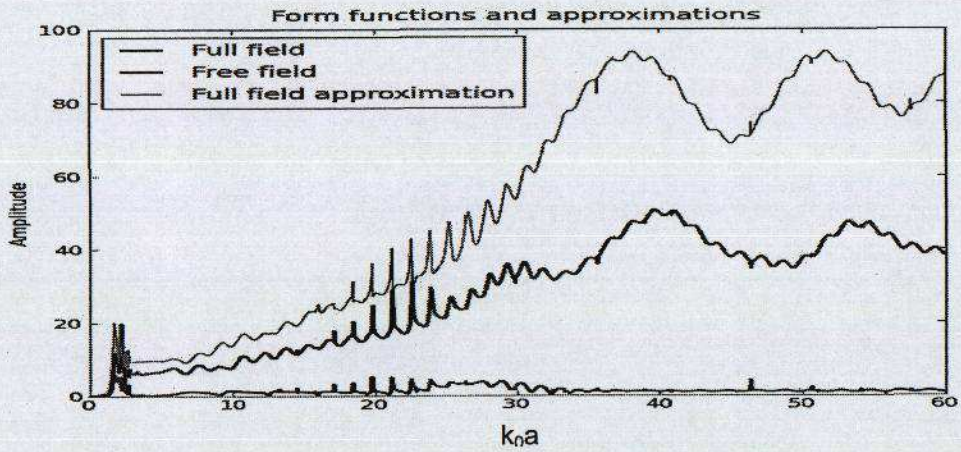

Figure 7. Computation of the form functions for a shell placed 1mm beneath the interface, alpha =0°

In Figures 6 and 7 it is clearly seen that the frequency response of an object close to an interface is very different from the scattered field of the same object in free field conditions. Arising differences are due to interactions between the object and interface and between sound wave and interface. These effects depend strongly on both frequency and angle of incidence. They depend also on the distance between sphere and interface. If this distance tends to infinity, there are no more interactions with the interface and the scattered field is just the free field of the object. In Figures 6 and 7 we give also the results of an approximation of the full field (green curve). This approximation defined by Eq. (15) seems to be relatively acceptable for alpha =30° but it is not correct for alpha=0°. Its domain of validity should be studied in detail in the future.

4.1 Comparison Theory-Experiment

In order to check the full field computation, an experiment was carried out in the tank with the same spherical shell as before. The shell was placed beneath the air-water interface being very close to this interface. Different depths of immersion and different angles of incidence were successively studied. Moreover, in order to study the influence of strong resonances of the shell, two wide band Panametrics transducers, working respectively at 250 kHz and 500 kHz were used. A comparison between the experiment and theory can be observed in Figure 8 for transducer T2 (500 kHz). This transducer is working in the frequency domain corresponding to strong resonances of the object. The echoes obtained for two different angles of incidence (Figures 8a and 8b) have a very complex structure resulting from strong interactions between interface and object. If we compare modelling and experiment, the general agreement is quite good. In particular, the position of different components of

the echoes is well predicted by modelling but as before, small differences in signal amplitude can still be observed.

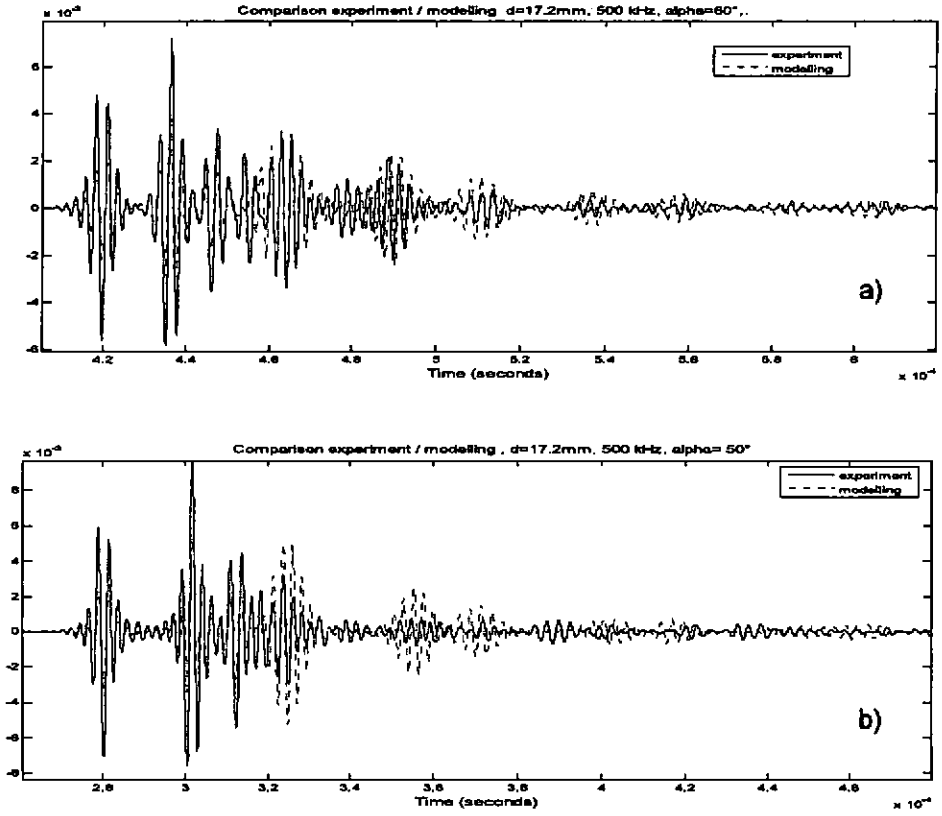

Figure 8. Echoes of the shell close to the air-water interface: a) α =60°; b) α =50°

Frequency: 500 kHz, r/a~20

In the case of transducer T1 (250 kHz), the frequency range covered by this transducer does not allow excitation of strong resonances. Figure 9 shows an example of echo for the incidence angle of 50°. This signal has a simpler structure than the one shown in Figure 8b. If we compare modelling and experiment, the general agreement is again satisfactory. In particular, the position of different components of the echoes is well predicted by modelling.

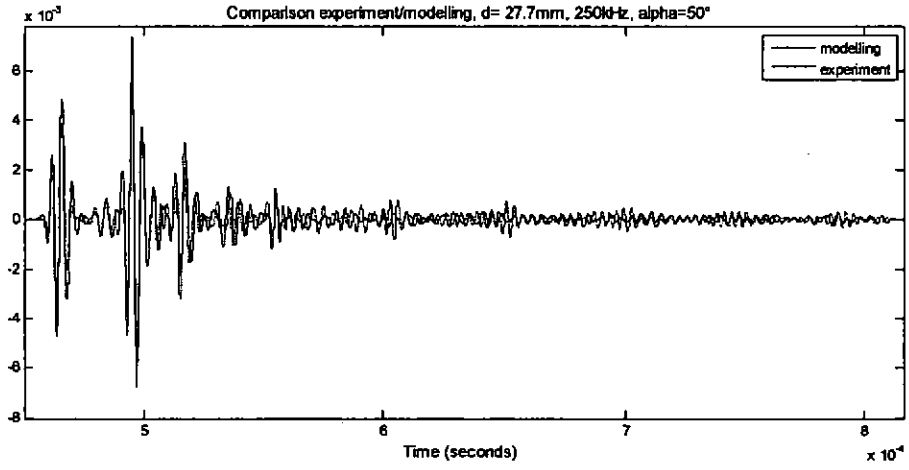

Figure 9. Echo of the shell close to the air-water interface, α =50°

Frequency: 250 kHz, r/a~20

5 DISCUSSION OF THE RESULTS

5.1 Comparison Between a Free Field Echo and an Echo with Interface Interactions

This comparison has been made for transducers T1 and T2. Figure 10 gives the result of comparison for transducer T1 (250 kHz). The two curves have been obtained from experimental data. We can observe that the presence of the air-water interface modifies significantly the structure of the free field echo. This modification of the echo by the environment becomes even more important in the case where strong resonances of the object are excited by transducer T2 (500 kHz). This case is shown in Figure 11.

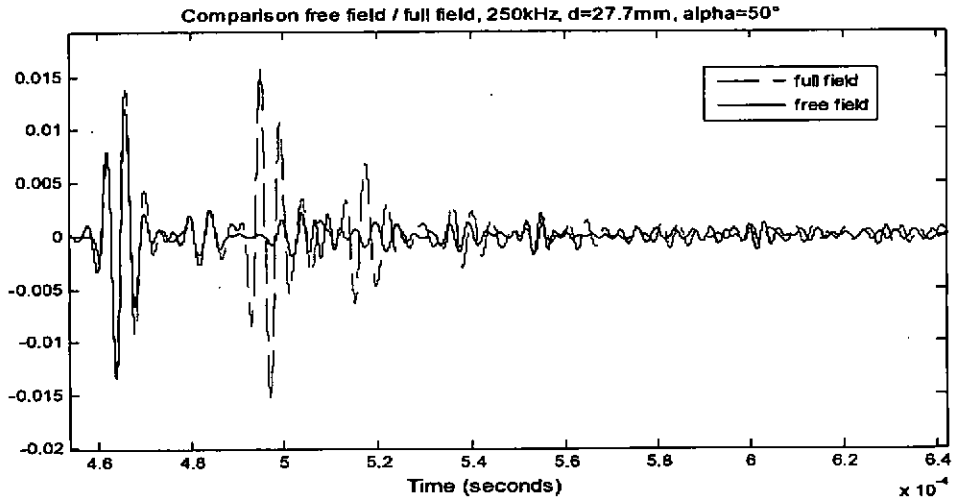

Figure 10.Comparison free field / full field, transducer T1 (250 kHz)

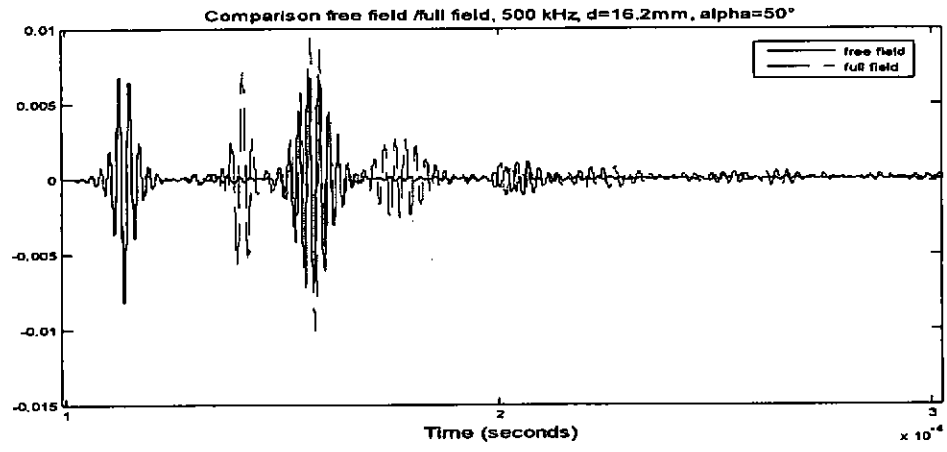

Figure 11. Comparison free field / full field, transducer T1 (500 kHz)

5.2 Geometrical Interpretation of Different Arrivals

In order to understand the structure of the echoes in the situation where the object is close to an interface, and in the most complex situation corresponding to the case, where A_0 waves were excited, we used the ray theory. This simple approach can be used to predict the arrival times of signal components due to:

- direct reflections by the object,
- successive reflections by interface and object,
- surface waves of the A_0 type after different circumnavigations on the shell surface,
- different reflections of these surface waves on the air-water interface.

Different ray paths used for the computation of travel times are shown in Figure 12.

The results of these computations are shown in Figure 13. We can see a good agreement between the arrival times predicted by the ray theory and different components of the signal which have been clearly identified.

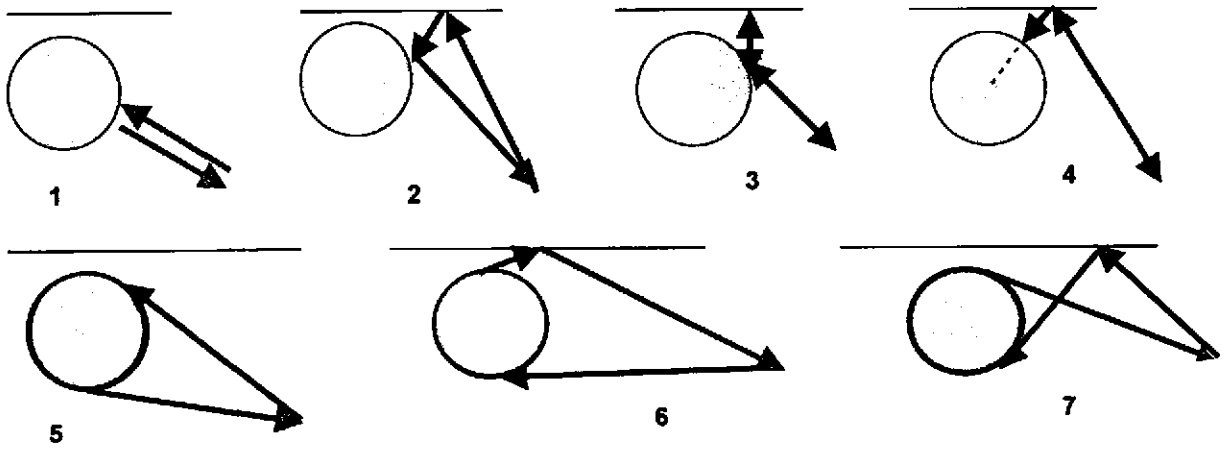

Figure 12. Rays paths used for calculation of different travel times

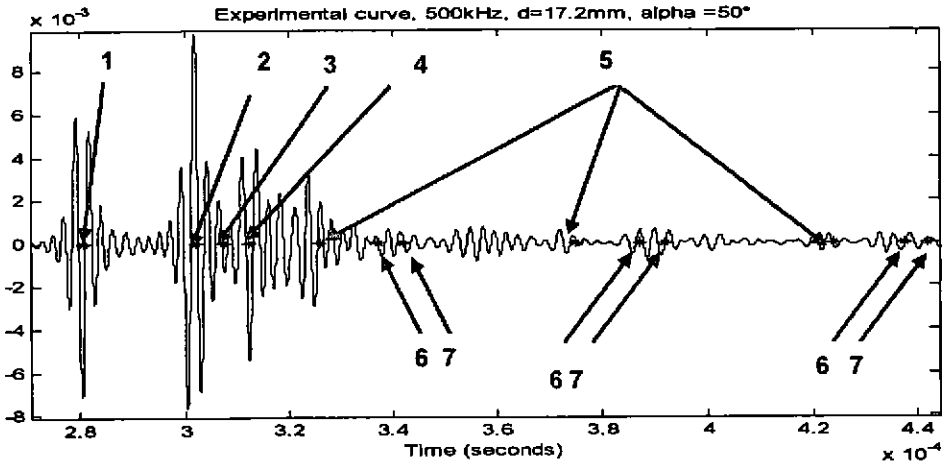

Figure 13. Arrival times of different components of a signal calculated by the ray theory

6 CONCLUSION

The results presented in this paper confirm the strong influence of the air-water interface on the scattering by an elastic shell placed just beneath this perfectly reflecting interface. This influence depends on several parameters; among them the distance between an object and boundary, the angle of incidence and the frequency content of the transmitted signal. It was shown that in the resonance regimes of the elastic shell, strong interactions due to surface waves can take place and in these conditions it becomes very difficult to identify the target. All the obtained results were confirmed by tank experiments performed in well controlled conditions. Moreover, we showed that even in a complex case where there are a lot of interactions, the arrival times of different components of the echoes can be predicted by the ray theory.

It should be noted that these results can be extended without too many modifications to the case of an object close to a water-fluid bottom interface.

7 REFERENCES

1. H. Huang and G.C Gaunaurd, "Acoustic point source scattering by a spherical elastic shell submerged beneath a free surface", J. Acoust. Soc. Am. 99, 2720-2726 (1996).
2. R.H Hackman and G.S Sammelmann, "Multiple-scattering analysis for a target in an oceanic waveguide", J. Acoust. Soc. Am. 84, 1813-1825 (1988).
3. J.A. Fawcett and R. Lim, "Evaluation of the integrals of target/seabed scattering using the method of complex images", J. Acoust. Soc. Am. 114, 1406-1415 (2003).
4. S.G. Kargl and P.L. Marston, "Ray synthesis of Lamb wave contributions to the total scattering cross section for an elastic spherical shell," J. Acoust. Soc. Am. 88, 1103-1113 (1990).
5. R. Lim, J.L. Lopes, R.H Hackman, and D.G. Todoroff, "Scattering by objects buried in underwater sediments: Theory and experiments", J. Acoust. Soc. Am. 93, 1762-1783 (1993).
6. G.C. Gaunaurd and H. Huang, "Acoustic scattering by a spherical body near a plane boundary", J. Acoust. Soc. Am. 96, 2526-2536 (1994).
7. A. Messiah, "Clebsch-Gordan (C.G.) coefficients and 3j symbols," Appendix C.I in Quantum Mechanics, Vol 2, 1054-1060, North-Holland, Amsterdam, The Netherlands, (1962).